



Tailored alumina nanocomposite membranes featuring MIL-125-NH₂ metal-organic frameworks for oily wastewater treatment



Umair Baig ¹✉, Abdul Waheed ¹, Lukka Thuyavan Yogarathinam¹ & Isam H. Aljundi ^{1,2}✉

Ceramic membranes offer significant potential for addressing challenging and harsh wastewater streams such as produced water (PW) and surfactant-stabilized oil/water (O/W) emulsions. This study focuses on developing a stable and a uniformly structured active layer solely composed of MIL-125-NH₂ MOF on a ceramic Alumina support. A stable covalent bonding approach was employed using interfacial polymerization, with isophthaloyl chloride (IPC) acting as the organic crosslinker during interfacial polymerization reaction. Three distinct MIL-125-NH₂ decorated membranes M50, M75, and M100 were prepared by using varying MOF concentrations. Surface wettability analysis of the membranes indicated that the MIL-125-NH₂ MOF active layer displayed super-hydrophilic characteristics in the air (water contact angle = 0°) and super-oleophobic characteristics underwater (oil contact angle = 161.5°). In oil separation experiments, all the MIL-125-NH₂ deposited membranes displayed >99% oil rejection. Among the fabricated membranes, M50 demonstrated the highest water flux of 2100 Lm⁻² h⁻¹ under a transmembrane pressure of 2 bar. The MIL-125-NH₂ MOF deposited membranes also showed stable performance under longer-run filtration. This study would be a simple and effective method of decorating MOFs as an active layer on ceramic support for efficient O/W emulsion separation and desalination applications.

The quality of water in natural resources such as lakes, rivers, and seas is deteriorated by the marine oil spills and discharge of oily wastewater from a variety of industries, including the petroleum, pharmaceutical, metal processing industries, and food. Such oily wastewater exists in the form of oil in water (O/W) emulsion or immiscible oil-water mixture, both of which are harmful to the environment and eventually human beings^{1,2}. Membrane technology has been demonstrated to be more effective and sustainable than traditional treatment methods for the treatment of oily wastewater in large-scale industrial applications³. Ceramic membranes are the preferred choice of membrane materials for various industrial wastewater treatments due to their innate characteristics, which encompass hydrophilicity, remarkable mechanical robustness, and chemical stability^{3,4}. The effectiveness of O/W separation relies on a membrane's resistance to fouling which is the buildup of unwanted substances such as oil, particles, or organics on the membrane's

surface or within its pores. Hydrophilic membranes are frequently an ideal choice for O/W emulsion separation⁵. However, oil droplets stabilized by surfactants readily adhere to the membrane surface via the hydrophilic portions of the surfactant, leading to pore blockage and diminishing the efficiency and effectiveness of the separation process, resulting in decreased flux and heightened energy consumption⁶. Surface modification of ceramic membranes has garnered recent attention in the pursuit of developing hydrophilic surfaces with oleophobic properties for the enhancement of performance of oil-water separation.

Metal-organic frameworks (MOFs) are porous materials formed through the coordination of metal ions or clusters with organic ligands, resulting in a highly ordered, crystalline structure with an expansive internal surface area. MOF-based membranes, combining the features of MOFs with membrane structures, possess significant promise in a range of industries

¹Interdisciplinary Research Centre for Membranes and Water Security, King Fahd University of Petroleum and Minerals, Dhahran 31261, Saudi Arabia.

²Chemical Engineering Department, King Fahd University of Petroleum and Minerals, Dhahran 31261, Saudi Arabia. ✉e-mail: umairbaig@kfupm.edu.sa; aljundi@kfupm.edu.sa

due to their tunable characteristics, extensive surface areas, defined pore sizes, antifouling tendency, and selective capabilities^{7,8}. MOF membranes are becoming increasingly attractive for O/W separation due to their hydrophilic and underwater oleophobic properties⁹. Titanium (Ti) centered MOFs are highly appealing because of the presence of a tetravalent cation that exhibits excellent redox capabilities and forms robust metal-ligand bonds within a stable framework. MIL-125-NH₂ is a porous 3D amine functionalized Ti-based MOF containing octahedral and tetrahedral cages within its structure¹⁰. Lately, Zhu et al. decorated a MIL-125-NH₂@polyacrylic acid layer on the polyvinylidene fluoride (PVDF) substrate using vacuum deposition to enhance the separation of O/W emulsion¹¹. The MIL-125-NH₂@polyacrylic acid membrane exhibited consistent and outstanding rejection performance, along with notable flux capabilities, even after 10 filtration cycles. Wang et al. decorated the MIL-125-NH₂ hybridized reduced graphene oxide on cellulose acetate film through self-assembly for the treatment of oily wastewater and dye solution¹². The resulting membrane displayed outstanding resistance to fouling, as well as resistance to both acidic and alkaline conditions, while maintaining a rejection rate of 99% and a flux of more than 600 Lm⁻² h⁻¹. MIL-125-NH₂ demonstrated a highly effective membrane layer in achieving a high flux without compromising the rejection for O/W separation. Since MIL-125-NH₂ has a huge potential for O/W emulsion separation, we have chosen MIL-125-NH₂ to be decorated as a stable active layer onto a ceramic support for the O/W emulsion separation.

Generating a stable and continuous selective layer composed of MOFs on a microfiltration support such as ceramic alumina support is a considerable challenge. Any defect that emerges during fabrication of membrane has the potential to hinder the inherent separation abilities of these membranes¹³. The deposition of MOFs in ceramic membranes can be achieved through various techniques such as the formation of a MOF layer or coating on the ceramic membranes surface, the infiltration of MOF nanoparticles through the ceramic porous structure¹⁴. The commonly adopted methods for fabricating MOF membranes are in-situ growth, layer-by-layer deposition, solvothermal reactions, seed-assisted secondary growth, electrospinning, vacuum-assisted filtration, and electrodeposition^{13,14}. Although such techniques are promising, these techniques have certain limitations such as expensive instrumentation, tedious fabrication procedures, and large-scale production. Moreover, the majority of the membranes prepared by these techniques have been applied in dead-end configuration in lab scale experiments. In addition, most of the MOF-based membranes have been prepared by mixing MOFs as fillers in the polymeric matrix without a stable bonding which could be washed out during filtration experiments. Therefore, the need of the day is to develop a highly stable and continuous MOFs active layer supported by a ceramic microfiltration support which can be effectively applied in a crossflow filtration mode. Given the high utility and versatility of interfacial polymerization in membrane fabrication, interfacial polymerization (IP) can be readily applied for generating a stable and defect-free active layer on a support. IP is a well-established technique which has been widely used on the industrial scale. During IP, an active layer is generally grown using an aqueous amine and non-aqueous acid chloride on an ultrafiltration(UF)/microfiltration(MF) support. IP has shown positive effect in integration of MOFs as fillers in thin film nanocomposite (TFN) nanofiltration (NF), reverse osmosis (RO), and forward osmosis (FO) membranes¹⁵⁻¹⁸.

Owing to the presence of a free amino group (-NH₂) per each ligand in MIL-125-NH₂ MOF structure, MIL-125-NH₂ MOF is an ideal candidate for IP reaction. There are several amino groups in the structure of MIL-125-NH₂ which can effectively take part in Schotten Baumann reaction with acid chloride groups of a crosslinker. Due to a reaction between the amino group (-NH₂) of MIL-125-NH₂ MOF and acid chloride group (-COCl) of a crosslinker, a stable amide bond (-CONH) is formed leading to a continuous and stable active layer in the membrane. Hence, the current work is dedicated to developing a highly stable, uniform and defect-free active layer composed of MIL-125-NH₂ MOF decorated on an alumina ceramic

support by IP reaction where MIL-125-NH₂ was reacted with isophthaloyl chloride (IPC). The resultant MIL-125-NH₂ MOF membrane was tested for its O/W surfactant stabilized emulsion separation by installing the membranes in a crossflow filtration mode. The concentration optimization of MIL-125-NH₂ MOF was achieved by fabricating three membranes using three different MOFs containing membranes. These membranes were extensively characterized by using all the relevant membrane characterization techniques and subsequently testing the membranes by using a feed prepared by emulsifying crude oil in the water. Different parameters for establishing the O/W emulsion separation potential of the MIL-125-NH₂ membranes were studied and optimized in the current study.

Results and discussion

The MIL-125-NH₂ MOF was synthesized by using an amino-functionalized ligand ATPA and TTIP as a metal source (Fig. 1a). The ATPA ligand was purposely selected in this study to eventually get a MOF with an inbuilt amino (-NH₂) functional group so that it can readily take part in reaction with IPC during the interfacial polymerization reaction. This approach will yield an active layer composed of well-decorated MIL-125-NH₂ MOF on the surface of alumina ceramic support (Fig. 1b).

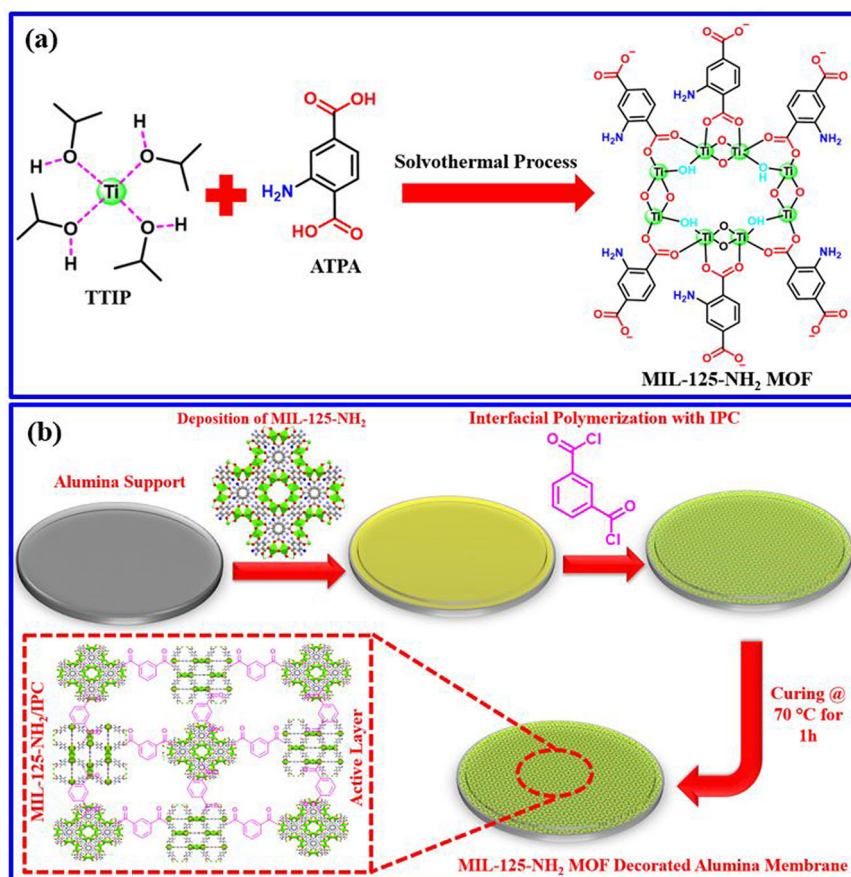
Characteristics of MIL-125-NH₂ MOF

As seen in Fig. 2a and Supplementary Figure 1, distinct and intense diffraction peaks were observed for the MIL-125-NH₂ MOF at 2θ angles of 6.89°, 9.85°, and 11.75°, corresponding to the crystallographic planes of (0 1 1), (0 0 2), and (1 2 1), respectively¹⁹. The FTIR spectrum of MIL-125-NH₂ MOF (Fig. 2b) revealed the chemical structure by recording the characteristics peaks owing to the presence different constituents. The most prominent peak was observed at around 3400 cm⁻¹ which was observed as doublet of peaks which is a characteristic of a primary amine (-NH₂). Hence, the amino (-NH₂) group of the ATPA was confirmed by FTIR. On moving further, another set of highly important peaks was found at around 3000 cm⁻¹ which is attributed to sp² C-H stretching of the benzene rings of ATPA. A peak confirming the carbonyl (>C=O) group of carboxylic groups (-COOH) was found to be located at 1532 cm⁻¹ (Fig. 2b). Hence, the structure of the organic linker ATPA was completely confirmed by FTIR. The binding of the Titanium metal with carboxylate groups was confirmed due to the existence of several Ti-O-Ti stretching vibrations at the wavenumbers of 774 cm⁻¹, 639 cm⁻¹, and 514 cm⁻¹^{20,21}.

The surface morphology of MIL-125-NH₂ MOF resembles thin disc-like structures with an estimated average particle size of 0.7 μm arranged in uniform order (Fig. 2c-e). EDX analysis confirmed the presence of all the constituent elements including titanium (Ti), oxygen (O), carbon (C), and nitrogen (N) (Fig. 2f). The elemental mapping revealed a uniform spatial distribution of all the constituent elements throughout the structure of the synthesized MIL-125-NH₂ MOF. The presence of these elements is attributed to different reaction participants including TTIP and ATPA. The content of each element in the MIL-125-NH₂ MOF is reflected by the density of the mapping dots in the respective mapping image (Fig. 4g-j). The highest C content among all the elements is a confirmatory indication of the participation ligand ATPA which is further confirmed by N owing to the presence of amino groups (-NH₂) in ATPA.

Figure 3a shows the N₂ adsorption/desorption isotherm of the synthesized MIL-125-NH₂ MOF. The isotherm analysis showed type I isotherm at 77 K with no hysteresis phenomenon. The calculated BET surface area was 965 m²/g. In the low relative pressure region, the adsorption curve increases sharply which indicates the presence of micropores. The adsorption curve reached a plateau after that indicating that most of the MOF porosity is attributed to the micropores. The calculated surface area and volume of the micropores was 723 m²/g and 0.282 cc/g, respectively. Figure 3b shows the pore size distribution of the synthesized MOF. The pore width (mode) was 0.889 nm with an average pore diameter of 1.7 nm. The total pore volume at relative pressure of 0.926 was 0.341 cc/g indicating that more than 80% of the pores are micropores. The adsorption isotherms of N₂ on MIL-125-NH₂ reveal intriguing behavior, particularly its high

Fig. 1 | Proposed scheme for the synthesis of MIL-125-NH₂ MOF and its decorated membrane. **a** The chemical reaction for the synthesis of MIL-125-NH₂ MOF using an amino-functionalized ligand ATPA and TTIP as a metal source via the solvothermal process. **b** Various phases involved in the fabrication of the MIL-125-NH₂ MOF decorated alumina ceramic membrane using an interfacial polymerization process.



adsorption capacity at low partial pressures. However, within a wide range, the adsorption amount exhibits only insignificant changes until reaching saturation pressure, where it rapidly increases. This phenomenon can be elucidated by considering the energy distribution of adsorption sites within the MOF structure and the presence of multiple peak energy distribution functions^{22,23}. At low partial pressures, the availability of vacant adsorption sites allows for efficient adsorption of N₂ molecules, resulting in high adsorption capacity. As the partial pressure increases, the competition for these adsorption sites becomes more pronounced, leading to diminishing changes in adsorption amount. However, at saturation pressure, additional adsorption sites may become accessible due to structural rearrangements or cooperative interactions between N₂ molecules and the MOF framework, resulting in the observed increase in adsorption capacity. Figure 3c–f shows various structures of the MIL-125-NH₂ MOF exhibiting different orientations along various planes and symmetries showing the porosity of the synthesized MIL-125-NH₂ MOF.

Decoration of MIL-125-NH₂ active layer on alumina support

Given the presence of amino groups in the linker ATPA, the MIL-125-NH₂ MOF can be efficiently decorated as an active layer through the Schotten Baumann reaction between the amino groups of MIL-125-NH₂ MOF and acid chloride groups of IPC. Hence, MIL-125-NH₂ MOF was successfully decorated on the ceramic support through stable covalent bonding between the MOFs units which is a highly desirable feature for membrane-based separations. Figure 4a shows the interfacial polymerization reaction and proposed active layer structure of MIL-125-NH₂ MOF grown on ceramic alumina support.

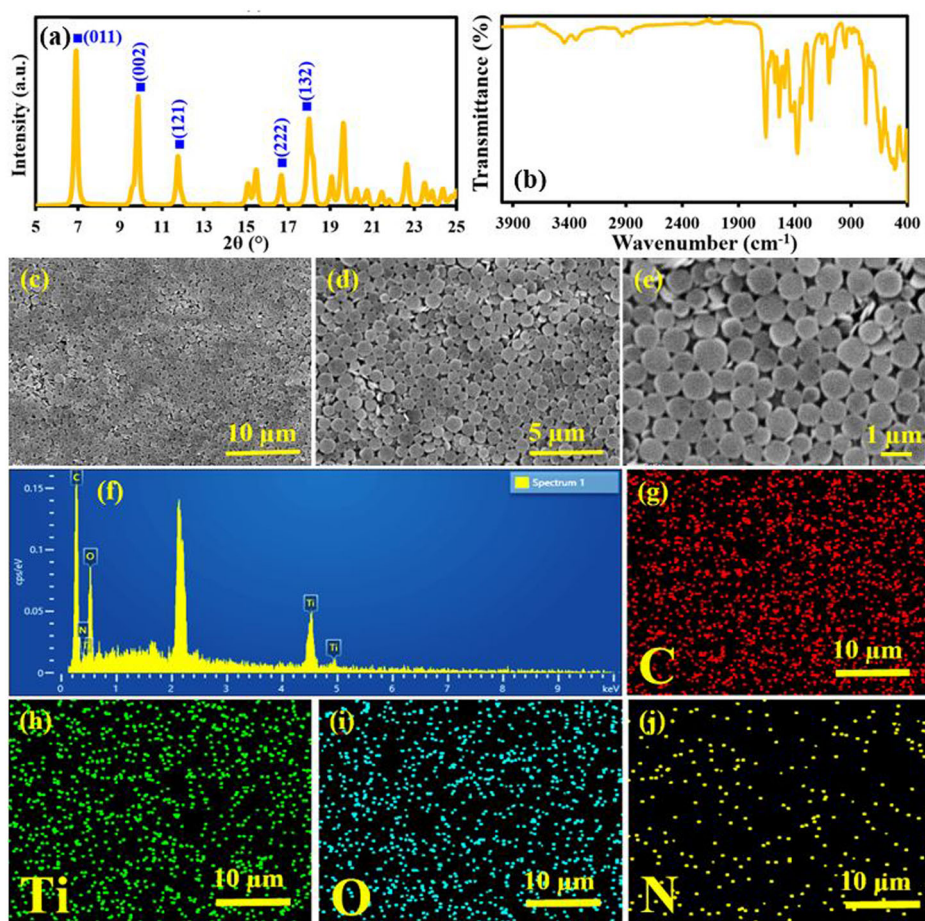
Surface chemistry & crystallinity analysis of MOF-membranes

Figure 4b shows the FTIR spectra of alumina support, M50, M75, and M100 nanocomposite membranes. As seen in Fig. 4b, the characteristic peaks of

alumina support correspond to Al–O stretching at 459, 595, and 656 cm⁻¹, while a peak at 900 to 1100 cm⁻¹ is attributed to the Al–O stretching vibration due to free surface hydroxyl groups (O–H) present at the surface of the membrane²⁴. The characteristic peaks of MOF functional groups are clearly identified in all the MIL-125-NH₂ MOF decorated alumina nanocomposite membranes. The characteristics peaks confirming the successful interfacial polymerization were identified at 3500 cm⁻¹ due to N–H stretching vibration of amide linkage (–CONH). A careful comparison of the amide peak of MIL-125-NH₂ MOF/IPC decorated membrane and amino groups of MIL-125-NH₂ MOF clearly shows a marked difference. In the case of MIL-125-NH₂ MOF, the peak at around 3500 cm⁻¹ is a doublet which is a characteristic of a primary amine while in the case of MIL-125-NH₂ MOF ceramic membrane, the amide bond shows a broad single band. The prominent spectra indicating the asymmetric (C=O) and symmetric carbonyl (C=O) stretching vibrations at 1532 cm⁻¹ and 1378 cm⁻¹ are distinctly present, confirming the successful polymerization of MIL-125-NH₂ MOF on the alumina substrate surface. Moreover, vibrations associated with Ti–O–Ti (774 cm⁻¹) are evident in the spectra. The intensity of MIL-125-NH₂ MOF became more pronounced as the decoration concentration increased from 50 mg/100 ml to 100 mg/100 ml.

Figure 4c shows the XRD pattern of alumina support, M50, M75, and M100 nanocomposite membranes. As seen in Fig. 4c, all the membranes displayed distinctive and prominently pronounced peaks corresponding to the crystallographic planes of alumina, specifically (116), (024), (113), and (104), which were observed at 2θ angles of 59.2°, 54.1°, 45.1°, and 36.9°, respectively. The observed peaks for the crystalline alumina align closely with those reported in the open literature²⁵. In the case of MIL-125-NH₂ MOF decorated alumina nanocomposite membranes, the additional MOF crystalline peaks were seen on the M50, M75, and M100 nanocomposite membranes. In all the nanocomposite membranes, the planes of MIL-125-NH₂ MOF with indices (132) and (222) were observed at 2θ angles of 18.5°

Fig. 2 | Crystalline structure, spectroscopic, morphological, EDX, and elemental mapping analysis of MIL-125-NH₂ MOF. a XRD pattern of MIL-125-NH₂ MOF, 2 θ range from 5 to 25°. **b** FTIR spectrum of MIL-125-NH₂ MOF, wavenumbers range from 400 to 4000 cm⁻¹. **c–e** SEM images of MIL-125-NH₂ MOF at three different magnifications. **f** EDX spectrum and **g–j** elemental mapping images for C, Ti, O, and N of MIL-125-NH₂ MOF.



and 16.9°, respectively. The intensities of prominent peaks of alumina were decreased due to the covering of the alumina support by MIL-125-NH₂ MOF. An obvious finding was an increase in the intensities of the peaks due to MIL-125-NH₂ MOF owing to increasing concentration of MIL-125-NH₂ MOF from M50 to M100. This justifies the fact that the interfacial polymerization reaction has resulted in the establishment of a considerable layer of MIL-125-NH₂ MOF onto alumina ceramic support.

Morphological analysis of membranes

Figure 5 shows the surface morphology analysis of alumina support, M50, M75, and M100 nanocomposite membranes. As seen in Fig. 5a–c, alumina support showed the porous structure with a considerably rough surface, irregular shaped alumina particles with a non-uniform particle size distribution. Since alumina support is microporous, numerous micro-sized pores and voids are evident in the entire membrane area. This porous arrangement, with a size of 0.1 μm , could potentially result in the passage of oil and subsequent pore clogging during the filtration process²⁶. A marked variation in the surface texture and surface morphology was observed upon successful interfacial polymerization reaction between MIL-125-NH₂ MOF and IPC onto alumina support. A thin layer composed of disc-shaped MIL-125-NH₂ MOF crystals with uniformly distributed pores was seen in the case of M50 (Fig. 5d–f), M75 (Fig. 5g–i), and M100 (Fig. 5j–l) membranes. Another important observation highlights the pore narrowing in the cases of M50, M75, and M100 when compared to the alumina support. The pores exhibited increased narrowing with increased concentration of MIL-125-NH₂ MOF. This pore constriction is a desirable feature required for rejecting the micro-sized oil droplets while allowing the water to permeate through the membranes under the applied feed pressure.

Figure 6 shows the EDX and mapping analysis of a representative M75 membrane. As anticipated from the membrane chemistry described in the

previous sections, EXD analysis revealed the presence of all the constituent elements including Ti, C, O, and N owing to the constituents of MIL-125-NH₂ MOF decorated as an active layer on ceramic alumina support (Fig. 6a, b). Smaller concentrations of other elements such as Al and Si were also observed which can be attributed to the components of alumina ceramic support. The mapping analysis exhibited a uniform distribution of all the elements detected by EDX analysis. The percentage concentration of each element in the MOF containing active later is reflected by the density of the mapping dots shown in their respective maps shown in Fig. 6c, h. When compared, the percentage of C, O, Ti, and N was higher than that of Al and Si which confirmed the presence of MIL-125-NH₂ MOF active layer on alumina support.

Wettability and porosity analysis of membranes

The membrane surface wettability is of immense importance in determining the O/W emulsion separation capability of a membrane. It has been observed in literature that membranes with underwater superoleophobic surfaces have an exceptional capability for separating the oil from water even in the case of surfactant stabilized O/W emulsion. Figure 7a shows surface contact angle analysis of M75 nanocomposite membranes in different media which include water, air, oil in air, and oil underwater. The water in air ($\theta_{W,A}$) and oil in air ($\theta_{O,A}$) contact angles were measured as 0°, which clearly depicted that the M75 membrane is both super-hydrophilic and super-oleophilic in air. This can be attributed to the surface chemistry of the MIL-125-NH₂ MOF decorated M75 membrane which has several hydrophilic groups such as -COOH, NH, -CONH, and OH along with hydrophobic moieties such as phenyl rings of ATPA organic linker. The hydrophilic groups develop a considerable interaction with water molecules such as strong hydrogen bonding while the oil is attracted due to organophilic moieties of the MOF in the air medium²⁷. However, the most

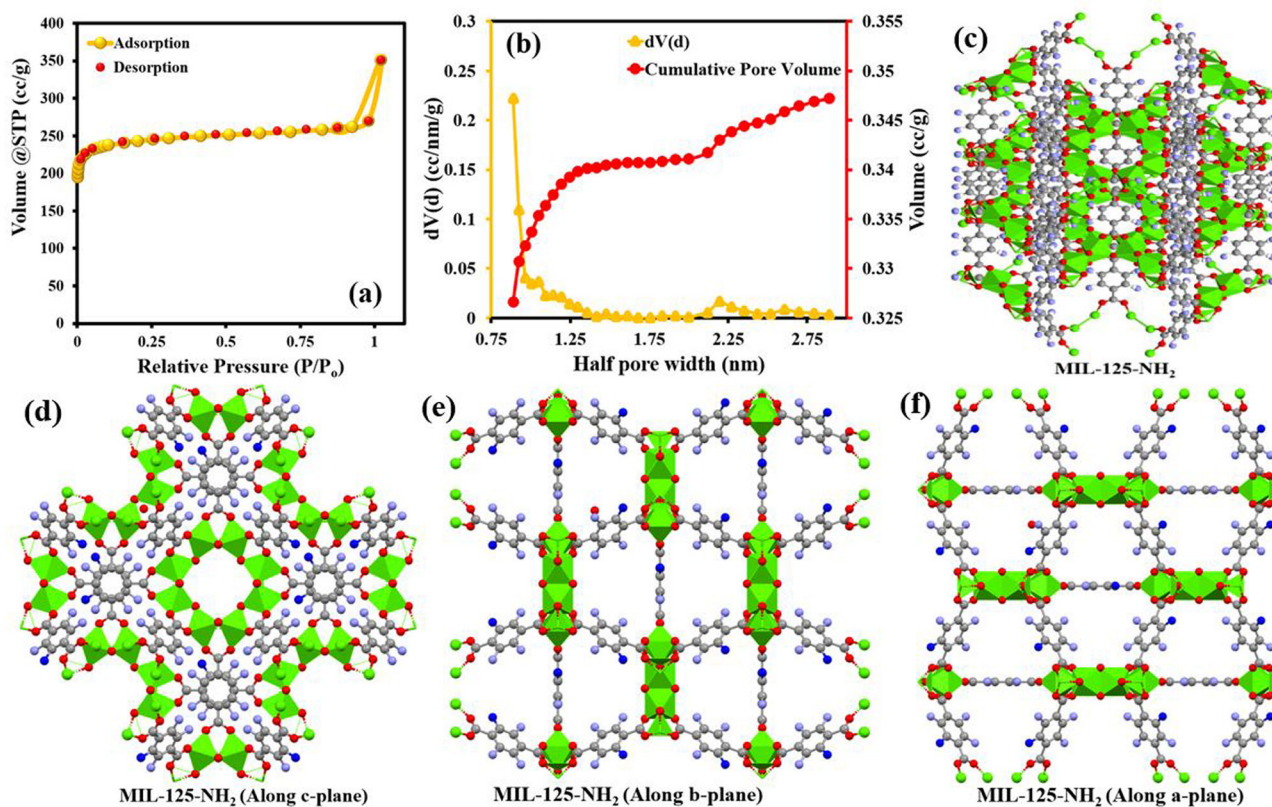


Fig. 3 | BET surface area analysis and 3D structures of the porous MIL-125-NH₂ MOF. **a** N₂ adsorption-desorption isotherm of MIL-125-NH₂ MOF and **b** Pore size distribution of MIL-125-NH₂ MOF. **c** 3D structures of the synthesized MIL-

125-NH₂ MOF. 3D structures of the synthesized MIL-125-NH₂ MOF along different planes: **d** along c-plane, **e** along b-plane, and **f** along a-plane.

important surface wettability is underwater surface chemistry which resembles the real-life filtration condition as the membrane is underwater during O/W separation experiments. A comparison of temporal contact angle measurements is also shown in Fig. 7b. The membrane was completely wetted with both water and oil in air in mere 2 s and 1 s, respectively. However, in the case of oil underwater contact angle measurements, oil-beading was observed which was found to be stable up to 2 min with an underwater contact angle measurement of 160.5°. This observation confirmed the fact that M75 has an underwater superoleophobic surface. This surface wettability of the membrane is attributed to the establishment of a strong hydration layer on the surface of the M75 membrane and such a phenomenon has also been observed with Strontium-MOF⁹. Such as surface wettability is an ideal feature required for O/W separation as the water is readily permeated through the membrane whereas the oil is rejected.

The bulk porosities (ϵ) of the M50, M75, and M100 membranes were also determined using a well-established procedure²⁸. The bulk porosities of the M50, M75, and M100 membranes were found to be 28.0%, 22.7%, and 21.5%, respectively.

Size distribution analysis of oil droplets in the surfactant stabilized crude oil-in-water emulsion has been carried out using Malvern Nano ZS Zetasizer as shown in Supplementary Figure 2. The average oil droplet size in the surfactant stabilized crude O/W emulsion was found to be ~95 nm.

Performance evaluation of membranes

Initially, the MOF-containing membranes were tested by measuring their water flux using DI water as feed in a crossflow filtration assembly. Figure 8a shows the water flux of M50, M75, and M100 membranes as a function of increasing transmembrane pressure where the pressure was increased from 0.5 to 2.0 bar. A linear correlation was observed between transmembrane pressure (TMP) and water flux. This correlation strongly suggests that the trend in flux aligns with the principles of Darcy's law. Among all the

fabricated membranes, M50 demonstrated the highest water flux of 2112 Lm⁻² h⁻¹ at a transmembrane pressure of 2 bar. The attainment of high flux under low transmembrane pressure can be attributed to a relatively higher porosity (28%) of the M50 membrane coupled with improved hydrophilicity owing to the presence of MIL-125-NH₂ MOF in the active layer. It is imperative to note that the flux gradually decreased as the decoration concentration of MIL-125-NH₂ MOF increased from 50 mg/100 ml to 100 mg/100 ml. It indicated that the higher concentration of decorated MIL-125-NH₂ MOF formed a dense layer over the alumina support under interfacial polymerization, leading to decrease in the porosities (22.7% and 21.4%) of the M75 and M100 membranes.

The oil/water emulsion separation experiments of the membranes were conducted by using a feed composed of 100 ppm aqueous solution of crude oil. Figure 8b, c shows the oil-water flux and rejection analysis of MIL-125-NH₂ MOF decorated alumina nanocomposite membranes M50, M75, and M100 as a function of varying transmembrane pressure ranging from 0.5 to 2.0 bar. Among the membranes, M50 displayed a flux of 963.4 Lm⁻² h⁻¹ and a separation efficiency of ~99% at a transmembrane pressure of 2.0 bar. The performance of M50 membrane could be due to the surface characteristics of being super hydrophilic in air and super-oleophobic characteristics under water. Since, the active layer of the membrane is composed of MIL-125-NH₂ MOF, several hydrophilic functional groups such as -CONH, -NH₂, and -COOH groups can develop a considerable hydrogen bonding between the MIL-125-NH₂ MOF active layer and water molecules yielding a strong hydration layer. Hence, the oil molecules are pushed away from the membrane surface due low adhesive force²⁹. The M75 and M100 membranes displayed permeate flux of 481.69 and 439.43 Lm⁻² h⁻¹ with separation efficiencies of 99.2% and 99.6%, respectively, at a transmembrane pressure of 2.0 bar. This observation can be attributed to the existence of a comparatively dense MIL-125-NH₂ MOF active layer as we moved from lower concentration to higher concentration of MIL-125-NH₂ MOF which resulted in

Fig. 4 | Decoration of MIL-125-NH₂ active layer on alumina ceramic support and their surface chemistry and crystallinity analysis. a Interfacial polymerization reaction between MIL-125-NH₂ MOF and IPC leading to an active layer composed of MIL-125-NH₂ MOF/IPC. **b** FTIR spectrum of bare alumina support, M50, M75, and M100 membranes ranging from 390 to 4000 cm⁻¹. **c** XRD pattern of bare alumina support, M50, M75, and M100 membranes ranging from 5 to 80°.

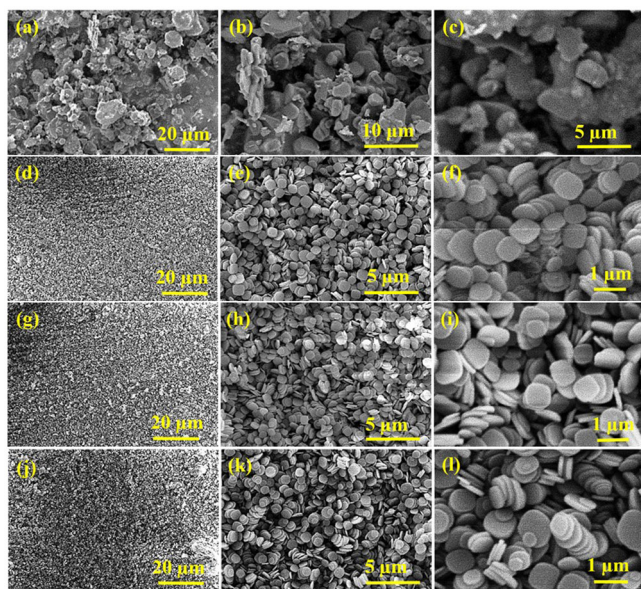
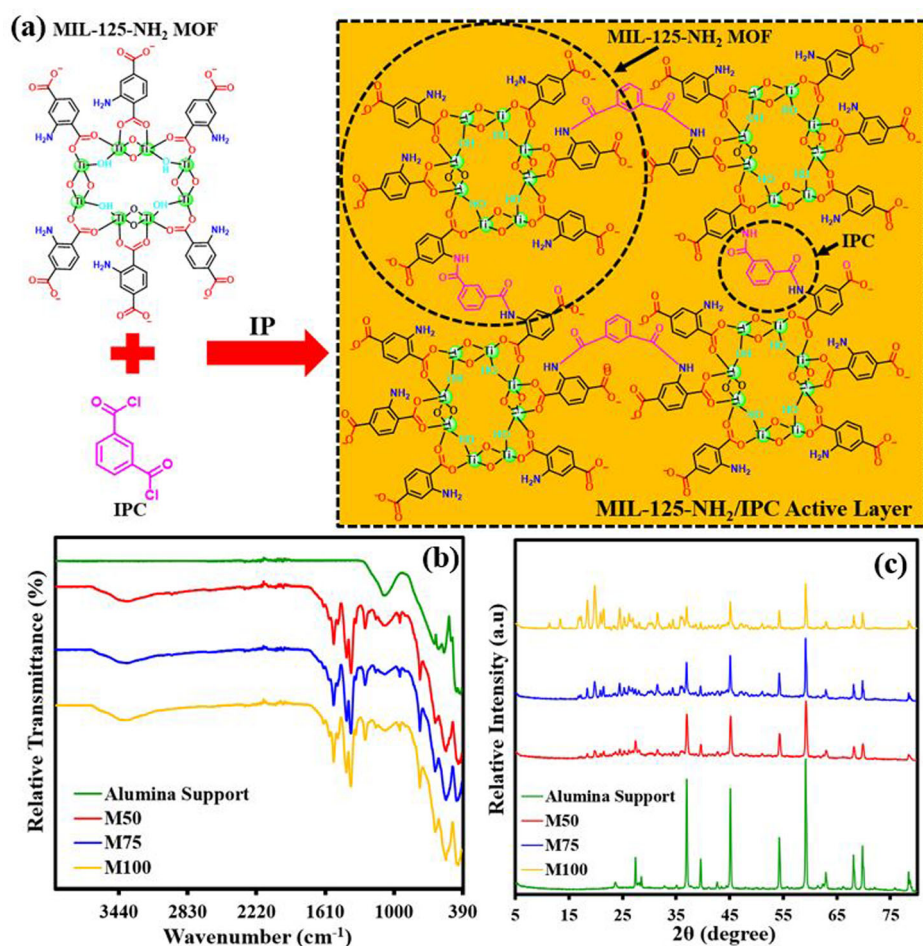


Fig. 5 | Surface morphological analysis of MIL-125-NH₂ MOF decorated alumina nanocomposite membranes. a–c SEM images of bare alumina support, M50 (d–f), M75 (g–i), and M100 membranes (j–l) at different magnifications.

narrowing of the pores as observed in the SEM analysis as well. Furthermore, all the membrane exhibited a superior rejection performance at the low transmembrane pressure of 0.5 bar. The decline in oil rejection was slightly mitigated under transmembrane conditions of 1.5 and 2.0 bar. This occurrence might be attributed to the diffusive force, leading to a flow of oil molecules across the surface.

Confirmatory evidence was collected from the digital and optical images of feed and permeate samples collected using M100 membrane at different TMPs as shown in Fig. 9. The feed appeared quite cloudy and milky confirming the formation of a stable emulsion having oil droplets completely emulsified by SDS surfactant. However, there were no visible oil droplets observed in the permeate, which indicated that the oil molecules were completely rejected by the MIL-125-NH₂ MOF active layer. For the sake of comparison, the separation performance of the bare alumina support was also measured as shown in Supplementary Figure 4. The separation efficiency of the bare alumina support was found to be 78% which is considerably lower compared to the MOFs decorated membrane. However, the most important finding of this experiment was that the separation of O/W emulsion was based on the adsorption of oil onto the surface of the alumina support. Owing the adsorption of oil on the alumina support a dramatic decrease in the permeate flux of the alumina support was observed. In comparison, the MOF-decorated membranes did not show any appreciable deposition of oil on the membrane surface. Digital images of the bare alumina support and MOF-decorated membrane M100 have been given in Supplementary Figure 5.

Fig. 6 | SEM/EDX and elemental mapping analysis of MIL-125-NH₂ MOF decorated alumina nanocomposite membrane (M75). **a, b** SEM/EDX analysis of M75 membrane and **c–h** elemental mapping images for C, O, Ti, Si, Al, and N of the M75 membrane.

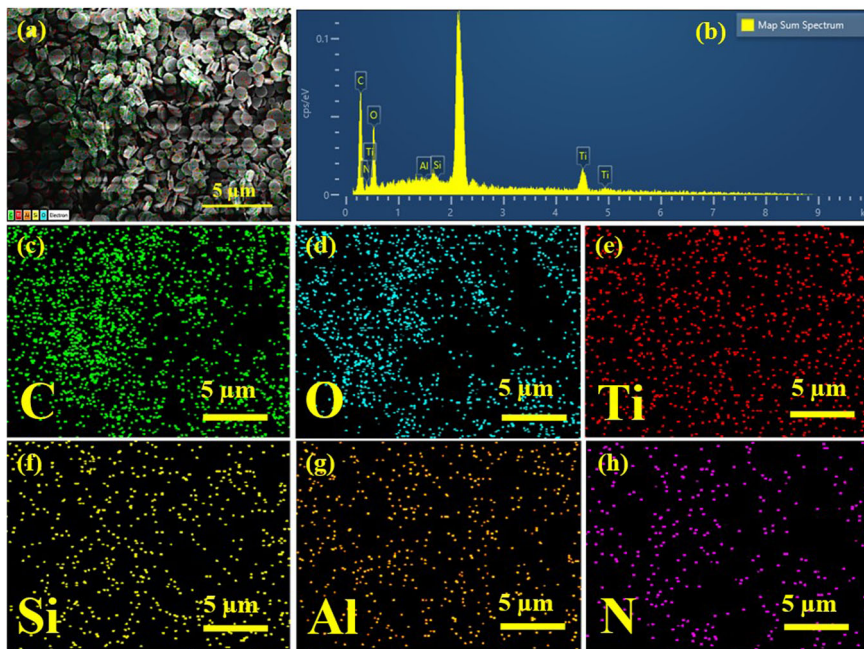


Fig. 7 | Wettability analysis of MIL-125-NH₂ MOF decorated alumina nanocomposite membrane. **a** Contact angle analysis of M75 membrane in different media such as water in the air, oil in the air, and oil underwater environment. **b** Temporal contact angle measurements of M75 membrane for water in the air, oil in the air, and oil underwater environment.

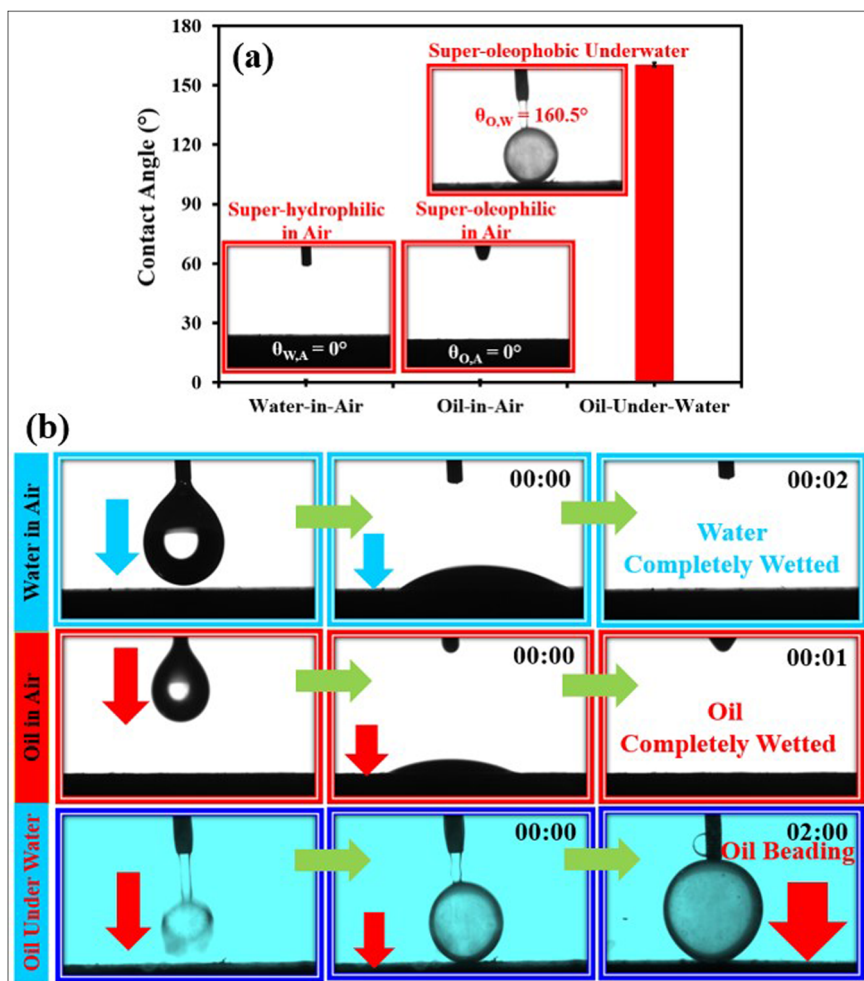


Fig. 8 | Water flux analysis and oil-in-water emulsion separation efficiency of the MIL-125-NH₂ MOF decorated alumina nanocomposite membranes. a Effect of pressure on pure water flux of MIL-125-NH₂ based membranes. Effect of pressure on permeate flux (b) and separation efficiencies (c) of MIL-125-NH₂ based membranes using 100 ppm crude oil-in-water emulsion as feed. The error bar represents the standard error.

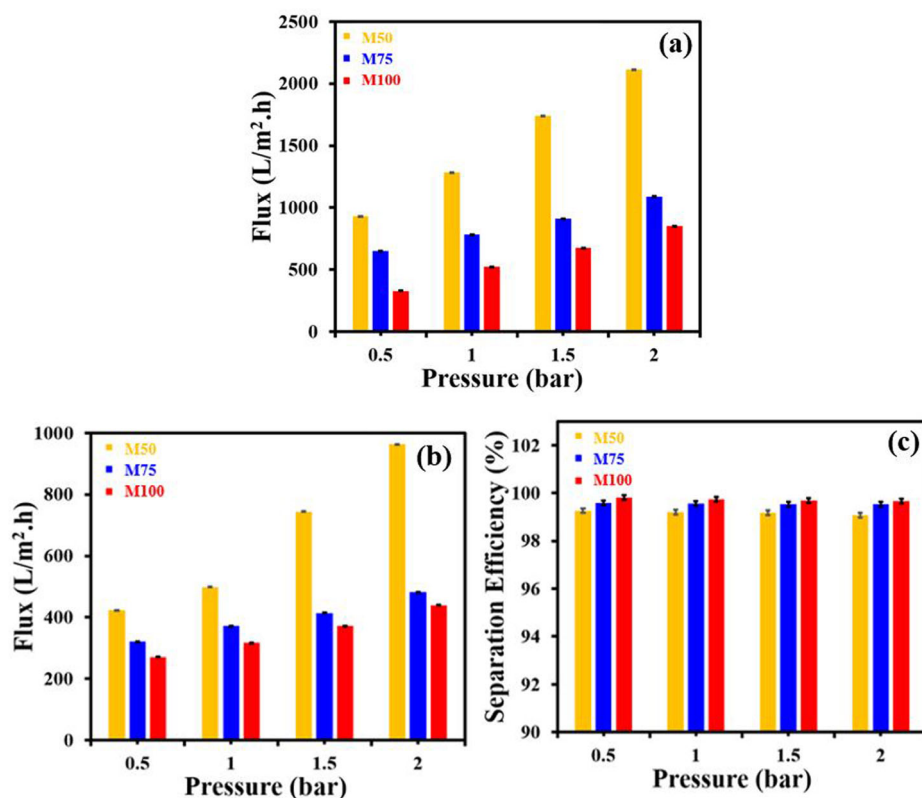
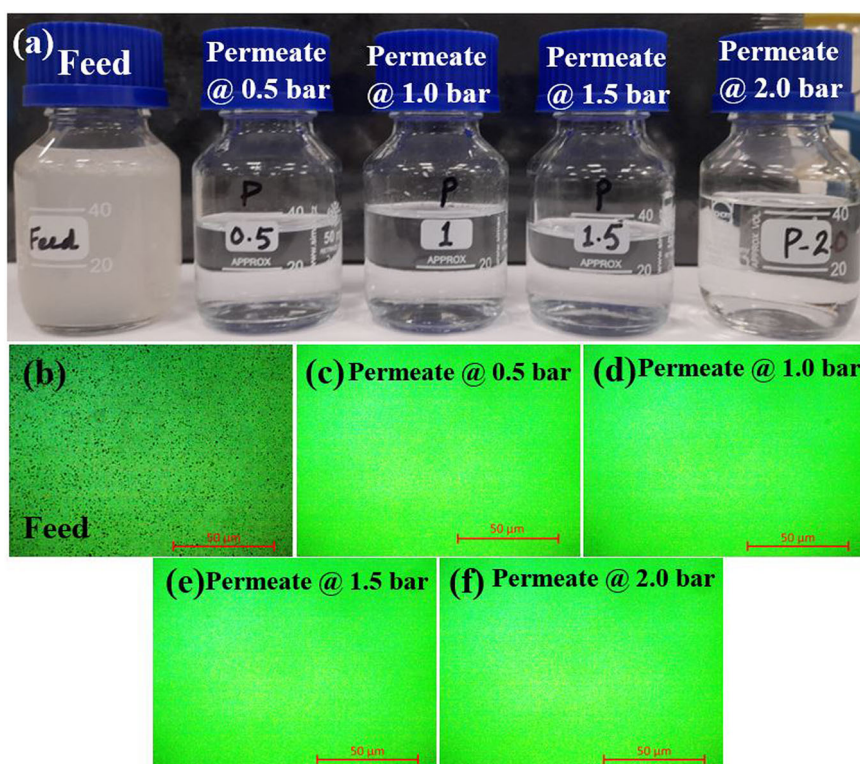


Fig. 9 | Digital and optical visualization of feed and permeate samples. a Digital and b–f optical images of the feed (100 ppm crude oil-in-water emulsion) and permeate samples were collected at different trans-membrane pressures using an M-100 membrane and crossflow filtration system.

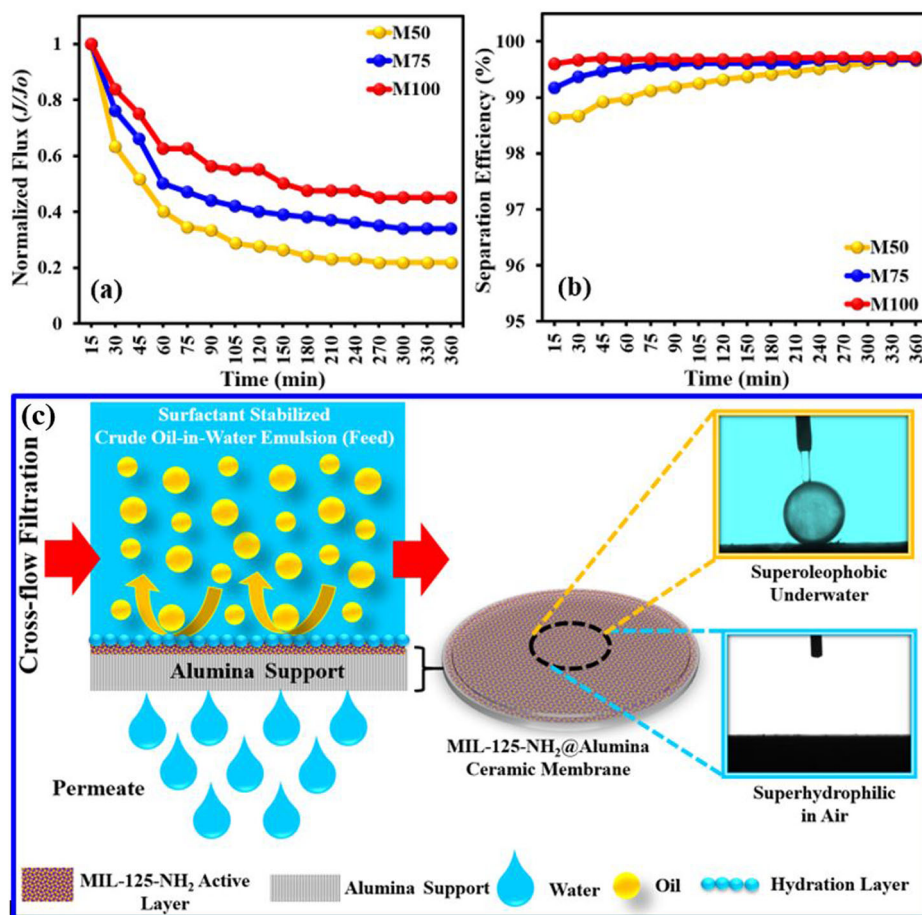


Long-term fouling analysis

The long-term stability of the membrane was studied by using 100 ppm crude O/W emulsion as feed. Figure 10a, b shows the long-term performance of the membranes M50, M75, and M100, illustrating the variations in

permeate flux and separation efficiency. As depicted in Fig. 10a, the flux decreases as time progresses and reaches a steady state in nearly 100 minutes. The initial decline in the permeate flux may be attributed to the gradual adherence of oil droplets on the membrane surface, which

Fig. 10 | Long-term fouling analysis and Oil-in-water emulsion separation mechanism of MIL-125-NH₂ MOF decorated alumina nanocomposite membranes. Permeate flux (a) and separation efficiencies (b) with time of MIL-125-NH₂ based membranes using 100 ppm crude O/W emulsion as feed. c Schematic sketch of surfactant stabilized crude O/W emulsion separation mechanism using super-hydrophilic and underwater super-oleophobic MOF-based ceramic membranes through crossflow filtration system.



eventually accumulates over time to form an oil layer. It relies on feed characteristics such as surfactant concentration, viscosity, and oil concentration³⁰. M100 membrane showed a lower decline in flux rate compared to other membranes. Over the extended filtration period of 360 min, the M100 membrane attained a normalized flux value of 0.45, while the M50 membrane underwent a decline, dropping to as low as 0.21. The low flux drop in M100 can be attributed to the formation of a dense MIL-125-NH₂ MOF layer with a stronger hydration layer compared to the M50 and M75 membranes which restricts the accumulation of oil droplets on the membrane surface lowering the membrane fouling. Furthermore, the M100 membrane exhibited a dense layer, as evident in the SEM analysis (Fig. 5). The following trend of declining flux was observed M50 < M75 < M100 (Fig. 10a). In terms of O/W emulsion separation, the separation efficiencies of the membranes gradually increased with decreasing flux which is obvious because of the well-known tradeoff between flux and rejection. The membranes showed a following decreasing trend of O/W emulsion separation M100 > M75 > M50 (Fig. 10b). In addition, we also performed the stability tests where the membranes were subjected to the O/W separation for 360 minutes and the performance of the membrane was monitored in terms of flux and separation efficiency. The flux was decreased during the first cycle with high separation efficiency. However, upon cleaning the membrane surface with methanol for 20 minutes by dipping the fouled membrane in clean methanol, the membrane was able to regain its performance. The cleaned membrane showed a flux recovery of 82% with an intact separation efficiency during the second cycle of performance analysis which highlighted the stability of the active layer deposited on the alumina ceramic support (Supplementary Figure 3).

The O/W emulsion separation mechanism of MIL-125-NH₂ MOF is illustrated in Fig. 10c. Given the underwater superoleophobic nature of the

membranes and the presence of several hydrophilic groups such as -COOH, -CONH, and -NH₂ a strong hydration layer is established on the membrane surface which inhibits the formation of an oil layer on the membrane surface. Hence, the oil is not able to wet the membrane and the oil is rejected by the membrane surface whereas the water is permeated through the membrane. Hence, the current approach is highly feasible for establishing an active layer of an amine-containing MOF on the ceramic support by interfacial polymerization reaction. The amino group enables the reaction of the MOF such as MIL-125-NH₂ with acid chloride groups of an appropriate crosslinker such as IPC. Therefore, a stable MOF active layer can be efficiently decorated for applications such as O/W emulsion separation and wastewater treatment.

The membrane performance was also compared the similar membranes from literature and tabulated in Table 1. The membranes prepared in the current study showed a comparable performance or better performance in some cases compared to the membranes known in literature. Although, the separation efficiency of the majority of the membranes known in literature is ≈98% but the flux is not as high as shown by the membranes prepared in the current study which is attributed to the salient features of the MIL-125-NH₂ MOF such as high surface area, porosity, and hydrophilic pores^{31–34}.

MIL-125-NH₂ MOF was successfully decorated as an active layer on alumina ceramic support through interfacial polymerization for the effective separation of surfactant stabilized emulsion. MIL-125-NH₂ characterization revealed a morphology resembling thin discs, featuring well-defined crystalline planes and the presence of hydrophilic groups. Surface morphology revealed that the thin disc-like MIL-125-NH₂ MOF layer were clearly visible on the surface of alumina ceramic support. EDX analysis confirmed the homogeneous dispersion of MOF elements on the ceramic membrane. The contact angle analysis of MIL-125-NH₂ MOF membrane exhibited a

Table 1 | Membrane performance evaluation with literature for oily-wastewater treatment

Membranes	Method	Oil in feed	Filtration mode	Surface wettability	Permeability (L m ⁻² h ⁻¹ bar ⁻¹)	Rejection (%)	Ref.
Coal fly ash (CFA)	Extrusion	Lubricating oil	Cross-flow	—	222.4	98.5	32
Zwitterionic carbon quantum dots (ZQDs)-cellulose acetate (CA)	Phase inversion	Diesel oil	Cross-flow	Water—54.7° Underwater oil—132.3°	350.5	98.9	33
Zwitterionic polydopamine/polyethyleneimine (PDA/PEI)-Al ₂ O ₃	Co-deposition	Soybean oil	Cross-flow	Water—11.81° Underwater oil—150.94°	40	98	34
pH responsive Dimethylaminopropylamine (DMAPA)-polystyrene maleic anhydride/ Polyvinylidene fluoride (PVDF)	Phase inversion	Crude oil	Cross-flow	Water—0° Underwater oil—150°	420	98.5	31
M50	Dead-end and interfacial polymerization	Crude oil	Cross-flow	Water—0° Oil—0° Underwater Oil—160.5°	498.59	98.64	This Study
M75					371.83	99.17	
M100					316.90	99.60	

superior super-hydrophilic (0°) and underwater super-oleophobic (160.5°) characteristics, an ideal feature for oil-water emulsion separation. Water flux analysis of MIL-125-NH₂ MOF membranes showed that the flux decreased with the increase of decoration concentration of MOF from 50 mg/100 ml to 100 mg/100 ml. A dense MOF layer was formed under higher decoration concentration of M75 and M100 membranes. In O/W emulsion separation studies, MIL-125-NH₂ MOF membranes showed more than 99% separation efficiency for the 100 ppm of crude oil emulsion. Long-term fouling depicted that the M100 MOF membrane outperformed with superior oil rejection and normalized flux, owed to higher decoration concentration of MIL-125-NH₂ MOF. Overall, this study would offer valuable insights into the design of MOF-based membranes using MIL-125-NH₂ for the O/W emulsion separation application.

The cost of synthesized MIL-125-NH₂ MOF and its based membrane were also estimated. The cost for the synthesis of MIL-125-NH₂ MOF is about US\$3.771/g, and the total cost for the fabrication of the MIL-125-NH₂ MOF-based membrane of 47 mm diameter is about US\$ 4.4533 and the breakdown of the cost is summarized in Supplementary Table 1. Also, the cost comparison for the fabrication of our MIL-125-NH₂ MOF-based membrane with that of commercial ceramic membranes is made in Supplementary Table 2, and it is quite clear that the former is more economical.

Methods

Chemicals and reagents

Titanium isopropoxide (TTIP), 2-aminoterephthalic acid (ATPA), Iso-phthaloyl chloride (IPC), methanol, N,N-dimethyl formamide (DMF), n-Hexane, were purchased from Sigma (USA). The Al₂O₃ ceramic supports were purchased from HIGHBORN New Materials Co., LTD. in China.

Synthesis of MIL-125-NH₂ MOF

MIL-125-NH₂ MOF was prepared by solvothermal approach using ATPA as an organic linker and TTIP as a metal source. Initially, 0.56 g ATPA was dissolved in 70 mL of DMF:Methanol mixture in a ratio of 9:1 followed by the addition of 0.6 mL TTIP and the reaction mixture was stirred for 20 minutes at room temperature. Then the reaction mixture was transferred into a Teflon-lined stainless-steel autoclave, sealed, and kept in a heating oven at 150 °C for 24 hours. After 24 hours, the autoclave was removed from the oven and allowed to cool down where MIL-125-NH₂ MOF was obtained as a yellow precipitate. The yellow precipitate was thoroughly washed with excess of DMF and methanol to remove the residual reactants. The obtained MIL-125-NH₂ MOF was further refluxed in DMF for 2 hours followed by isolation using centrifugation. Finally, the MIL-125-NH₂ MOF was extensively washed with water and calcined at 200 °C for 6 h. The purified MIL-125-NH₂ MOF was extensively characterized and used for membrane fabrication. Figure 1a shows the chemical reaction for the synthesis of MIL-125-NH₂ MOF using the solvothermal process.

Fabrication of MIL-125-NH₂ MOF-based membranes

MIL-125-NH₂ MOF decorated alumina membranes were fabricated by the interfacial polymerization where the three different concentrations of MIL-125-NH₂ MOF were decorated on an alumina ceramic support. In a typical membrane fabrication procedure, an aqueous dispersion of MIL-125-NH₂ MOF was prepared by dispersing 50 mg of MIL-125-NH₂ MOF in 100 ml of distilled water and homogenized by probe sonicator for 15 min followed by filtration on the alumina support fixed in a dead-end-filtration cell (Sterlitech, Auburn, WA, USA). This led to deposition of MIL-125-NH₂ MOF onto the Al₂O₃ ceramic support and subsequently the MOF-deposited membrane was allowed to dry in open air. To stabilize the deposition of MIL-125-NH₂ MOF onto the alumina support, the dried membrane was dipped in 0.15% (wt/v) n-hexane solution of isophthaloyl chloride (IPC) for 30 minutes. The resultant membrane was washed with n-hexane to remove the unreacted IPC. Finally, the MIL-125-NH₂ MOF ceramic membrane was cured in an oven at 70 °C for 1 h and hence obtained membrane was labeled as M50. The other two membranes M75 and M100 were also prepared by using the same procedure except the concentration of MIL-125-NH₂ MOF

was 75 mg/100 mL and 100 mg/100 mL, respectively. Figure 1b shows the steps involved in the fabrication of the MIL-125-NH₂ MOF decorated alumina ceramic membranes.

Characterization

The crystal structure and order of the synthesized MIL-125-NH₂ MOFs and MIL-125-NH₂ MOFs decorated alumina membranes (M50, M75, and M100) were evaluated using X-ray diffraction (XRD, MiniFlex-600, Rigaku). The analysis employed copper K-alpha radiation with a wavelength of 1.542 angstroms and scanned a broad range of angles from 5 to 80 degrees. Preceding XRD investigation, meticulous drying, and micronization yielded homogeneous microcrystalline samples, subsequently mounted on the designated holder for optimal data acquisition. The surface functionalities of the synthesized MIL-125-NH₂ MOFs were characterized by Fourier transform infrared spectroscopy (FTIR, Nicolet iS-50, Thermo Fisher Scientific) FTIR employing KBr pellets within a scan wavenumber range of 390 to 4000 cm⁻¹. Similarly, the MIL-125-NH₂ MOFs decorated alumina membranes were also evaluated using attenuated total reflectance Fourier transform infrared (ATR-FTIR) spectroscopy. Prior to morphology analysis, synthesized MIL-125-NH₂ MOFs and MIL-125-NH₂ MOFs decorated alumina membranes were gold sputtered and analyzed using scanning electron microscopy coupled with Energy dispersive X-ray spectroscopy (SEM/EDX, Coxem EM-30AX SEM) at the voltage of 10 kV. The surface wetting/non-wetting properties of the MIL-125-NH₂ MOF decorated alumina membranes were evaluated using the sessile drop method to analyze contact angles of water and oil, employing a goniometer (KRUSS, DSA25). Water contact angle (WCA) measurements were carried out on the membranes in an air environment by depositing 2 μL droplets at various locations. The resulting contact angles were averaged and documented, providing a representation of the surface wettability. A similar procedure was employed for measuring the oil contact angle in an air environment, with a droplet concentration of 1 μL. Oil contact angle measurements were also conducted on the membrane in an underwater environment by directly injecting oil droplets onto the submerged membrane.

Filtration experiment

Crossflow module was used to evaluate the permeate flux and oil rejection of M50, M75, and M100 membranes. The performance analysis was investigated at different transmembrane pressures between 0.5 and 2 bar. The permeate flux (J) of each membrane was calculated using Eq. (1).

$$J = \frac{V}{A \times t} \quad (1)$$

where V , A and t are the permeate volume (L), membrane effective area (m²) and time (h), respectively. The stock solution of 1000 ppm O/W emulsion was prepared by mixing 1 g of crude oil in 1 liter of distilled water where 0.5 g of SDS was added as an emulsifying agent using a shear mixer set at 30,000 rpm. The stock solution was diluted with distilled water to prepare 100 ppm of crude O/W emulsion to be used as the feed solution during the separation experiments. The separation efficiencies of membranes were calculated using Eq. (2).

$$\text{Separation efficiency} = \left(1 - \frac{C_p}{C_f}\right) \times 100 \quad (2)$$

where C_p is the oil concentration in the permeate while C_f is the oil concentration in the feed.

Data availability

All data generated or analyzed during this study are included in this published article (and its supplementary information files).

Received: 20 November 2023; Accepted: 13 March 2024;

Published online: 01 April 2024

References

- Zhou, Q. et al. Geological evolution of offshore pollution and its long-term potential impacts on marine ecosystems. *Geosci. Front.* **13**, 101427 (2022).
- Abuhasel, K. et al. Oilywastewater treatment: overview of conventional and modern methods, challenges, and future opportunities. *Water* **13**, 980 (2021).
- Jiang, D. et al. Customized copper/cobalt-rich ferrite spinel-based construction ceramic membrane incorporating gold tailings for enhanced treatment of industrial oily emulsion wastewater. *Sep. Purif. Technol.* **320**, 124131 (2023).
- Hatimi, B. et al. Low cost pyrrhotite ash/clay-based inorganic membrane for industrial wastewaters treatment. *J. Environ. Chem. Eng.* **8**, 103646 (2020).
- An, Y. P. et al. Janus membranes with charged carbon nanotube coatings for deemulsification and separation of oil-in-water emulsions. *ACS Appl. Mater. Interfaces* **10**, 9832–9840 (2018).
- Zhang, J. et al. A comprehensive review on the behavior and evolution of oil droplets during oil/water separation by membranes. *Adv. Colloid Interface Sci.* **319**, 102971 (2023).
- Goh, S. H. et al. Metal–Organic Frameworks (MOFs)-based mixed matrix membranes (MMMs) for gas separation: a review on advanced materials in harsh environmental applications. *Small* **18**, 2107536 (2022).
- Li, J. et al. Metal-organic framework membranes for wastewater treatment and water regeneration. *Coord. Chem. Rev.* **404**, 213116 (2020).
- Raj, A. et al. Underwater oleophobic-super hydrophilic strontium-MOF for efficient oil/water separation. *Chem. Eng. J.* **453**, 139757 (2023).
- Abdul Mubarak, N. S. et al. The chemistry of MIL-125 based materials: structure, synthesis, modification strategies and photocatalytic applications. *J. Environ. Chem. Eng.* **10**, 106883 (2022).
- Zhu, X. et al. NH₂-MIL-125@PAA composite membrane for separation of oil/water emulsions and dyes. *Colloids Surf. A Physicochem. Eng. Asp.* **630**, 127542 (2021).
- Wang, J. et al. A super-hydrophilic NH₂-MIL-125 composite film with dopamine-modified graphene oxide is used for water treatment. *N. J. Chem.* **101**, 13303–13314 (2022).
- Cheng, Y. et al. Advances in metal-organic framework-based membranes. *Chem. Soc. Rev.* **51**, 8300–8350 (2022).
- Awwad, M. et al. MOF-based membranes for oil/water separation: status, challenges, and prospects. *J. Environ. Chem. Eng.* **11**, 109073 (2023).
- Wang, Y. et al. Construction of high performance thin-film nanocomposite nanofiltration membrane by incorporation of hydrophobic MOF-derived nanocages. *Appl. Surf. Sci.* **570**, 151093 (2021).
- Liu, Y. et al. Thin film nanocomposite membrane incorporated with 2D-MOF nanosheets for highly efficient reverse osmosis desalination. *J. Memb. Sci.* **653**, 120520 (2022).
- Lee, J. Y. et al. Metal-organic framework-based porous matrix membranes for improving mass transfer in forward osmosis membranes. *J. Memb. Sci.* **492**, 392–399 (2015).
- Aljundi, I. H. Desalination characteristics of TFN-RO membrane incorporated with ZIF-8 nanoparticles. *Desalination* **420**, 12–20 (2017).
- Muelas-Ramos, V. et al. Synthesis of noble metal-decorated NH₂-MIL-125 titanium MOF for the photocatalytic degradation of acetaminophen under solar irradiation. *Sep. Purif. Technol.* **272**, 118896 (2021).
- Abdelhameed, R. M. et al. Fabrication of ZIF-67@MIL-125-NH₂ nanocomposite with enhanced visible light photoreduction activity. *J. Environ. Chem. Eng.* **7**, 103194 (2019).
- Choe, J. N. et al. Visible- light responsive PPynt@NH₂-MIL-125 nanocomposite for efficient reduction of Cr(VI). *Colloids Surf. A Physicochem. Eng. Asp.* **636**, 128147 (2022).

22. Ng, K. C. et al. A universal isotherm model to capture adsorption uptake and energy distribution of porous heterogeneous surface. *Sci. Rep.* **7**, 10634 (2017).
23. Burhan, M. et al. A universal mathematical methodology in characterization of materials for tailored design of porous surfaces. *Front. Chem.* **8**, 601132 (2021).
24. Baig, U. et al. Photo-responsive Zinc Oxide-coated alumina ceramic membrane with super-wettable and self-cleaning features fabricated by single step RF magnetron sputtering for oily water treatment. *Process Saf. Environ. Prot.* **175**, 541–553 (2023).
25. Baig, U. & Waheed, A. Facile fabrication of ceramic-polymeric nanocomposite membrane with special surface wettability using amino decorated $\text{NH}_2\text{-SiO}_2\text{@SiC}$ nanopowder for production of clean water from oily wastewater. *Process Saf. Environ. Prot.* **171**, 694–704 (2023).
26. Zhao, Y. et al. Surface manipulation for prevention of migratory viscous crude oil fouling in superhydrophilic membranes. *Nat. Commun.* **14**, 2679 (2023).
27. Zhu, X. et al. Chemically stable $\text{NH}_2\text{-MIL-125(Ti)/Sep/PDA}$ composite membranes with high-efficiency for oil/water emulsions separation. *Colloids Surf. A Physicochem. Eng. Asp.* **646**, 128899 (2022).
28. Guo, Z. et al. Submicro-pore containing poly(ether sulfones)/polyvinylpyrrolidone membranes for high-temperature fuel cell applications. *J. Mater. Chem. A.* **3**, 8847–8854 (2015).
29. Hu, J. et al. Durable and super-hydrophilic/underwater super-oleophobic two-dimensional MXene composite lamellar membrane with photocatalytic self-cleaning property for efficient oil/water separation in harsh environments. *J. Membr. Sci.* **637**, 119627 (2021).
30. Tummons, E. et al. Membrane fouling by emulsified oil: a review. *Sep. Purif. Technol.* **248**, 116919 (2020).
31. Chen, J. et al. Superhydrophilic/underwater superoleophobic PVDF ultrafiltration membrane with pH-responsive self-cleaning performance for efficient oil-water separation. *Sep. Purif. Technol.* **330**, 125420 (2024).
32. Huang, H. J. et al. Porous ceramic membranes from coal fly ash with addition of various pore-forming agents for oil-in-water emulsion separation. *J. Environ. Chem. Eng.* **11**, 109929 (2023).
33. Carballo, G. V. et al. Incorporation of zwitterionic carbon quantum dots in cellulose acetate tubular membrane for oil/water separation. *Sep. Purif. Technol.* **337**, 126301 (2024).
34. Luan, W. et al. Effective construction of anti-fouling zwitterion-functionalized ceramic membranes for separation of oil-in-water emulsion based on PDA/PEI co-deposition. *J. Environ. Chem. Eng.* **10**, 108396 (2022).

Acknowledgements

Authors would like to acknowledge the support provided by the IRC-MWS through project # INMW 2406, King Fahd University of Petroleum and Minerals, Saudi Arabia.

Author contributions

Umair Baig: Conceptualization, investigation, visualization, data curation, methodology, writing—review & editing. Abdul Waheed: Conceptualization, investigation, visualization, data curation, methodology, writing—review & editing. Lukka Thuyavan Yogarathinam: Visualization, data curation, writing—original draft. Isam H. Aljundi: Conceptualization, investigation, visualization, supervision, data curation, methodology, writing—review & editing.

Competing interests

The authors declare no competing interests.

Additional information

Supplementary information The online version contains supplementary material available at <https://doi.org/10.1038/s41545-024-00321-w>.

Correspondence and requests for materials should be addressed to Umair Baig or Isam H. Aljundi.

Reprints and permissions information is available at <http://www.nature.com/reprints>

Publisher's note Springer Nature remains neutral with regard to jurisdictional claims in published maps and institutional affiliations.

Open Access This article is licensed under a Creative Commons Attribution 4.0 International License, which permits use, sharing, adaptation, distribution and reproduction in any medium or format, as long as you give appropriate credit to the original author(s) and the source, provide a link to the Creative Commons licence, and indicate if changes were made. The images or other third party material in this article are included in the article's Creative Commons licence, unless indicated otherwise in a credit line to the material. If material is not included in the article's Creative Commons licence and your intended use is not permitted by statutory regulation or exceeds the permitted use, you will need to obtain permission directly from the copyright holder. To view a copy of this licence, visit <http://creativecommons.org/licenses/by/4.0/>.

© The Author(s) 2024